Journal of Materials Chemistry C

ROYAL SOCIETY OF CHEMISTRY

PAPER

View Article Online
View Journal | View Issue

Cite this: J. Mater. Chem. C, 2023, 11, 5450

Solar cells sensitized by donor-linked concerted companion dyes†

Jiaxin Luo,[a] Yuqing Wang,[a] Shaojin Shi,[a] Yuankun Wu,[a] Taochun Ma,[a] Leyao Wang,[a] Glib Baryshnikov,[b] Xinyan Wu,*[a] Chengjie Li*[a] and Yongshu Xie*[a]

Recently, concerted companion (CC) dyes have been developed by covalently linking the acceptors of organic and porphyrin dye units. Herein, a new class of CC dyes **XW85** and **XW86** have been designed by linking the donors of porphyrin and organic dye units with C_6H_{12} and $C_{12}H_{24}$ chains, respectively. The DSSCs of **XW85** based on the I_3^-/I^- electrolyte show significant J_{SC} (17.20 mA cm^{-2}) and PCE (8.96%), and **XW86** exhibits higher J_{SC} (18.55 mA cm^{-2}) and PCE (9.76%), which are also higher than those of the corresponding cosensitization systems. However, the PCEs for **XW85** and **XW86** are lower than that of the acceptor-linked reference dye **XW76** despite the obviously larger dye adsorption amounts. Desorption studies reveal that the CC dyes may be either double-anchored or single-anchored, with the double/single anchoring ratios lying in a sequence of **XW85** (1.31) < **XW86** (1.88) < **XW76** (6.34), consistent with that of increasing PCE. These observations indicate that the non-adsorbed sub-dye unit cannot effectively contribute to electron injection, and thus relatively large mono-anchoring proportions for **XW85** and **XW86** result in their relatively low J_{SC}, and the difference between **XW85** and **XW86** indicates that a longer linking chain is beneficial for partially alleviating the unfavorable single anchoring, resulting in superior performance. The results indicate that the photovoltaic behavior for the CC dyes may be further enhanced by avoiding the unfavorable alignment of the two carboxyl groups in opposite directions and thus simultaneously anchoring the two carboxyl groups, which may be realized through more rational molecular design.

Received 5th December 2022,
Accepted 27th March 2023

DOI: 10.1039/d2tc05167b

rsc.li/materials-c

Introduction

The conversion and utilization of solar energy have attracted extensive attention because of the demand for energy consumption, carbon emission reduction, and environmental protection.[1] As a representative technique in the field of photoelectric conversion, dye-sensitized solar cells (DSSCs) have been considerably developed since the first report by Grätzel and O'Regan in 1991.[2–5] As an essential component of DSSCs, light absorbing sensitizers harvest sunlight and transfer the photogenerated electrons into the semiconductor (TiO_2). Various types of sensitizers, such as ruthenium-based complexes,[6,7] metal-free organic dyes,[8–14] and porphyrin dyes,[15–21] have been designed with the purpose of improving the photovoltaic performance.[22–25]

Although high power conversion efficiencies (PCEs) have been achieved for the DSSCs based on porphyrin dyes due to their excellent light-harvesting properties,[3,4,15,26–28] one of the main drawbacks for porphyrin sensitizers is the weak absorption in the green color region between the Soret and Q bands, which limits sunlight harvesting and the PCE.[29–32] To address this problem, a cosensitization strategy has been developed and extensively employed by using a porphyrin dye and an organic dye with complementary absorption to achieve panchromatic absorption and PCE improvement.[33–36] Despite the success in this respect, the optimization process of the cosensitization approach is somewhat complicated and it is challenging to control the distribution of the two dyes on the semiconductor interface.[37,38] Recently, we have developed a class of concerted companion (CC) dyes by covalently linking the organic dye and porphyrin dye units through flexible chains at the acceptor moieties.[15,39–41] For example, **XW76** has been constructed by linking the acceptors of two sub-dye units corresponding to **XW10** and **XL3** (Fig. 1a).[26,40] Notably, these dyes exhibit panchromatic absorption in the visible region, resulting in high efficiencies and long-term photostability because of the double anchoring effect.

It has been reported that the capability of suppressing charge recombination may be improved by linking two branches of

[a] Key Laboratory for Advanced Materials and Joint International Research Laboratory of Precision Chemistry and Molecular Engineering, Feringa Nobel Prize Scientist Joint Research Center, Frontiers Science Center for Materiobiology and Dynamic Chemistry, Institute of Fine Chemicals, School of Chemistry and Molecular Engineering, East China University of Science & Technology, Shanghai 200237, China. E-mail: yshxie@ecust.edu.cn, chengjie.li@ecust.edu.cn, xinyanwu@ecust.edu.cn

[b] Department of Science and Technology, Laboratory of Organic Electronics, Linköping University, Norrköping SE-60174, Sweden

† Electronic supplementary information (ESI) available. See DOI: https://doi.org/10.1039/d2tc05167b

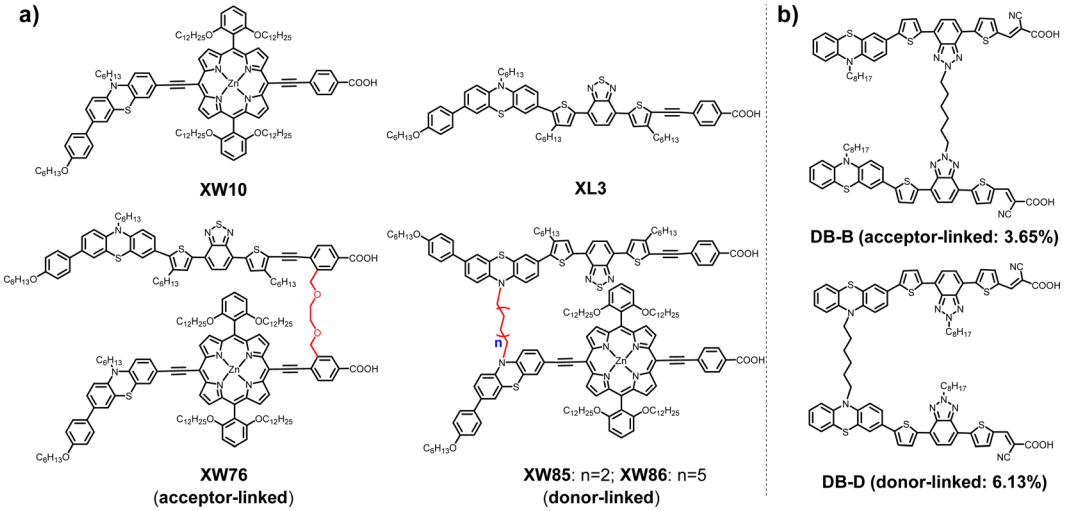

Fig. 1 Molecular structures of dyes (a) **XW10**,[26] **XL3**, **XW76**,[40] **XW85**–**XW86** and (b) **DB-B**, **DB-D**.[43]

organic dye units at the donor parts, and thus the photovoltaic performance may be enhanced (Fig. 1b).[42–46] Inspired by these results, the sub-dye units identical to those used for **XW76** have been employed to construct two novel CC dyes **XW85** and **XW86** by linking the phenothiazine donors with flexible chains of C_6H_{12} and $C_{12}H_{24}$, respectively (Fig. 1a).

As a result, **XW86** exhibits higher incident photon-to-current conversion efficiency (IPCE) plateau, larger J_{SC}, and higher PCEs (9.76% for I_3^-/I^- and 8.78% for $[Co(bpy)_3]^{3+/2+}$) compared to those of **XW85**. Notably, the PCE of **XW86** is also higher than those obtained by the cosensitizations of **XW10** and **XL3**. However, the PCE obtained for **XW86** is lower than that of the reference acceptor-linked CC dye **XW76**. The desorption behavior measurements have revealed that considerable amounts of dyes are singly anchored in the devices of **XW85** and **XW86**, which lowers the PCE of the cells. Compared with **XW85**, **XW86** with the longer linking chain affords an enhanced double/single anchoring ratio (1.88 for **XW86** *vs.* 1.31 for **XW85**), resulting in superior performance for **XW86**. The results indicate that the photovoltaic performance for CC dyes may be further improved by enhancing the double-anchoring proportion through elaborate molecular design in the future.

Results and discussion

Syntheses of the CC dyes

The synthetic procedures for the donor-linked CC dyes **XW85** and **XW86** are outlined in Scheme 1. Initially, the Suzuki

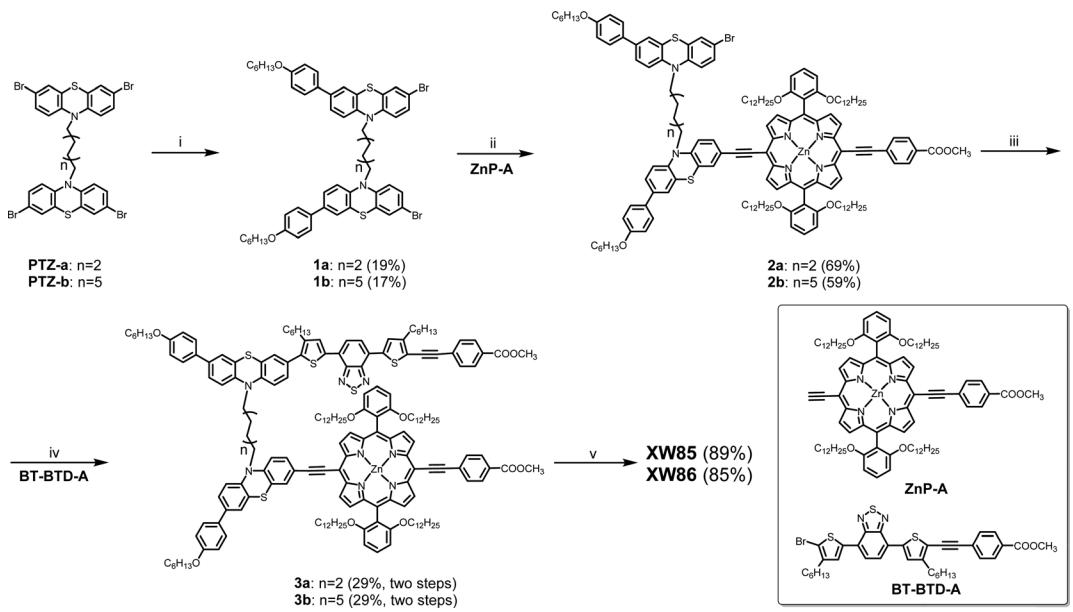

Scheme 1 Synthetic routes for **XW85**–**XW86**. Reaction conditions: (i) 4-(hexyloxy)phenylboronic acid, $Pd(PPh_3)_4$, K_2CO_3, THF, H_2O; (ii) $AsPh_3$, $Pd_2(dba)_3$, THF, Et_3N; (iii) bis(pinacolato)diboron, $Pd(PPh_3)_2Cl_2$, KOAc, 1,4-dioxane; (iv) $Pd(PPh_3)_4$, K_2CO_3, THF, H_2O; (v) $LiOH{\cdot}H_2O$, THF, H_2O.

coupling of diphenothiazine tetrabromides **PTZ-a** and **PTZ-b**[47] with 4-(hexyloxy)phenylboronic acid yielded the donor-attached dibromides **1a** and **1b**, respectively. Subsequent Pd-catalyzed Sonogashira coupling reactions with porphyrin alkynyl intermediate **ZnP-A**[48] produced **2a** and **2b**, respectively. Thereafter, Pd-catalyzed Miyaura coupling reactions of **2a** and **2b** with bis(pinacolato)diboron followed by Suzuki coupling with the organic dye acceptor unit **BT-BTD-A**[49] provided esters **3a** and **3b**, respectively, and then hydrolysis of the ester groups afforded **XW85** and **XW86**. The structures of all the synthesized compounds have been characterized by ^{1}H NMR, ^{13}C NMR, mass spectra, IR spectra and melting point (see the Experimental section and the ESI†).

Optical properties

The absorption spectra of the dyes in THF and anchored on thin TiO_2 films are presented in Fig. 2, with the corresponding data summarized in Table S1 (ESI†). Due to the structural similarity with the reported CC dye **XW76**, the donor-linked CC dyes **XW85** and **XW86** exhibit panchromatic absorption in the visible region similar to that of **XW76**.[40] The similar absorption characteristics of the three CC dyes indicate that the linking chain positions and lengths hardly perturb their light-harvesting capability. Upon anchoring onto the TiO_2 films, all the dyes show broadened bands (Fig. 2b), which can facilitate light-harvesting in the DSSCs.

To explore the possibility of energy transfer between the sub-dye units of the CC dyes, the emission spectra of the dyes have been measured. The porphyrin dye **XW10** and the organic dye **XL3** exhibit emission at 675 nm and 629 nm, respectively (Fig. S1a, ESI†), and the CC dyes **XW85**, **XW86**, and **XW76** demonstrate a strong emission peak at *ca.* 675 nm corresponding to the porphyrin unit (Fig. S1a and b, ESI†), with the peak at *ca.* 629 nm contributed by the organic dye unit considerably weakened, irrespective of the excitation wavelength (Fig. S1c, ESI†). These results are indicative of effective energy transfer from the organic dye unit to the porphyrin unit, which may partially compensate for the photocurrent loss for the singly anchored CC dyes *via* the porphyrin unit (*vide infra*).

Electrochemical properties

The electrochemical behavior of the CC dyes was investigated by cyclic voltammetry (CV) and differential pulse voltammetry (DPV) (Fig. S2, ESI†) to estimate the thermodynamic feasibility of the charge transfer processes. The energy level diagrams for the sensitizers, electrolyte redox potential, together with the conduction band edge of TiO_2 are shown in Fig. 3. The oxidation potentials (E_{ox}) of **XW85** and **XW86**, corresponding to their highest occupied molecular orbital (HOMO) levels, were found to be 0.83 and 0.80 V (*vs.* NHE), respectively, which are lower than the I_3^-/I^- and $[Co(bpy)_3]^{3+/2+}$ redox potentials (~0.4 V and 0.56 V *vs.* NHE, respectively) indicative of enough driving force for the reduction of the dye cations.[50] The optical band gaps (E_{0-0}) of **XW85** and **XW86** were both estimated to be 1.91 eV from the intersection of the normalized absorption and fluorescence spectra in THF. From the difference between the E_{0-0} and E_{ox} values, the excited state potentials were calculated to be −1.08 and −1.11 V (*vs.* NHE), considerably higher than that of the conduction band of TiO_2 (−0.5 V *vs.* NHE) suggesting that both of the sensitizers provide sufficient driving force for electron injection.

Photovoltaic performance

To evaluate the photovoltaic behavior of the donor-bridged CC dyes, the corresponding DSSCs have been fabricated using the I_3^-/I^- and $[Co(bpy)_3]^{3+/2+}$ electrolytes (see the ESI† for details). The photocurrent density–voltage (*J–V*) curves (Fig. 4a and c) and IPCE spectra (Fig. 4b and d) were measured under simulated sunlight (AM 1.5) and the corresponding photovoltaic

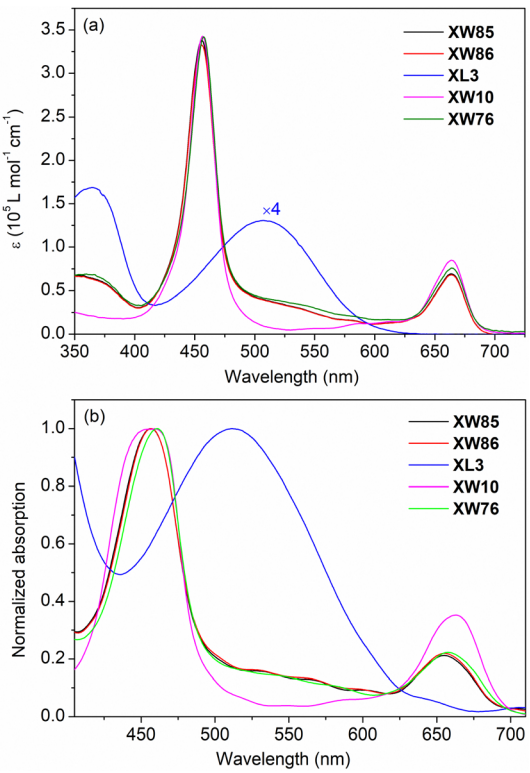

Fig. 2 Absorption spectra of the sensitizers (a) in THF, and (b) adsorbed on TiO_2 films (2 μm).

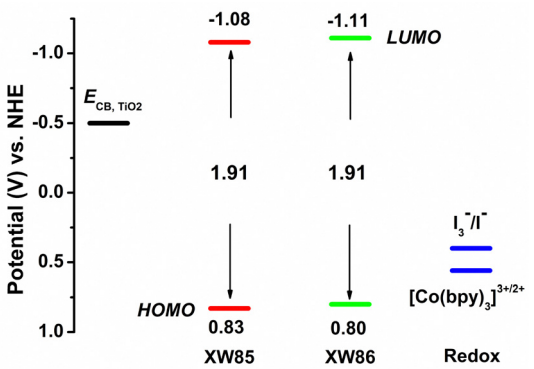

Fig. 3 Energy level diagrams of the sensitizers with respect to the conduction band of TiO_2 and the redox potentials of I_3^-/I^- and $[Co(bpy)_3]^{3+/2+}$.

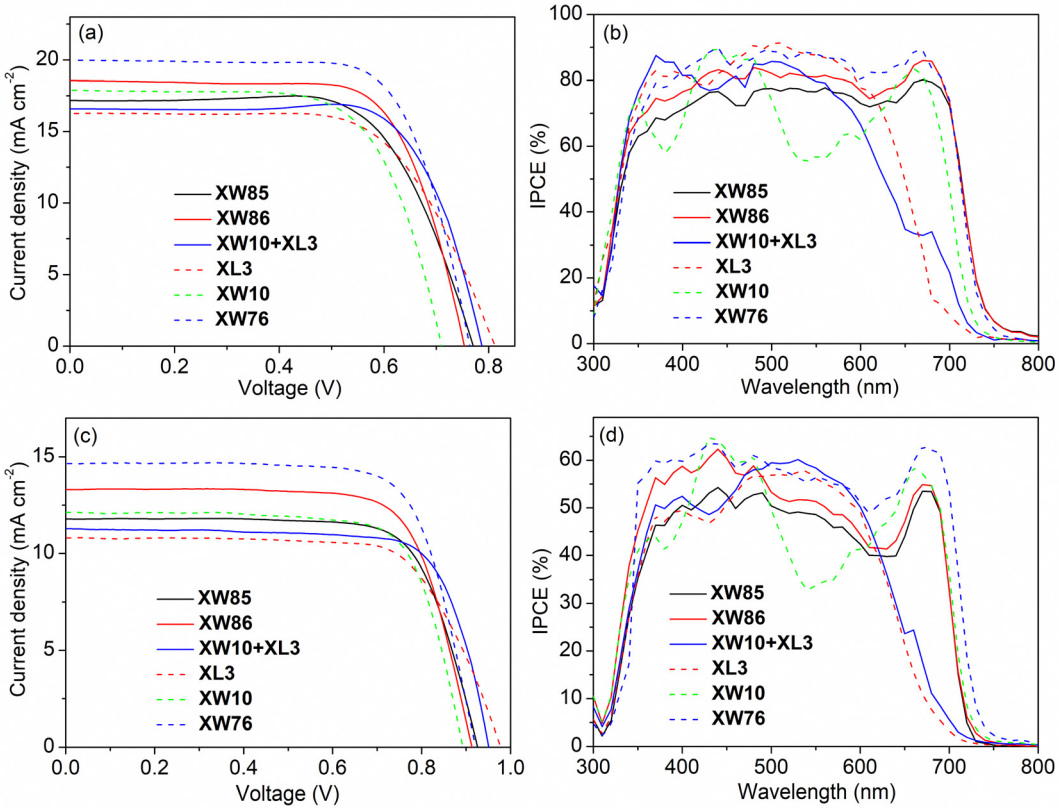

Fig. 4 *J–V* characteristic curves of the DSSCs using (a) iodine-based and (c) cobalt-based redox mediators, and IPCE spectra of the DSSCs using (b) iodine-based and (d) cobalt-based redox mediators.

parameters are collected in Table 1. For the DSSCs based on the I_3^-/I^- electrolyte, **XW85** exhibits V_{OC}, J_{SC}, and PCE of 767 mV, 17.20 mA cm^{-2}, and 8.96%, respectively. Compared with **XW85**, **XW86** exhibits a slightly decreased V_{OC} (755 mV) but an elevated J_{SC} (18.55 mA cm^{-2}), and the resulting PCE (9.76%) is higher than that of **XW85**. Compared to the corresponding component dyes **XL3** (PCE of 8.69%)[40] and **XW10** (PCE of 8.6%),[26] **XW85** and **XW86** show moderately improved photovoltaic performance. Furthermore, the efficiency achieved for **XW86** is higher than that of 9.28% obtained for the device cosensitized with **XW10** and **XL3**, which exhibits a considerably lower J_{SC} as a result of the considerably lowered adsorption amount of the porphyrin dye accompanied with the coadsorption of the organic dye (Table 1 and Table S2, S3, ESI†). Compared with the iodine-based DSSCs, the devices based on the cobalt electrolyte exhibit improved V_{OC} attributable to the higher potential of the cobalt redox mediator.[50] Despite the improved V_{OC}, the J_{SC} values are considerably lowered because of the mass transport limitation of the bulky cobalt complex.[51] As a result, **XW85** and **XW86** exhibit lowered efficiencies of 7.80% and 8.78%, respectively.

As illustrated in Fig. 4b and d, the IPCE spectra of **XW85** and **XW86** exhibit a panchromatic response over the visible region, similar to that of **XW76**. By integrating the IPCE data, J^{IPCE} values could be obtained, and they were found to be lower than the corresponding J_{SC} values obtained from the *J–V* tests by 0.5%–12.3% (Table 1 and Fig. S4, ESI†). These results may be rationalized by the fact that the full irradiation applied in the *J–V* test generates more heat and electrons, resulting in higher charge transport and collecting efficiencies, and thus higher J_{SC} values were obtained in the *J–V* tests.[30] Compared with the IPCE of **XW85**, **XW86** presents an elevated plateau, consistent with its higher J_{SC}, indicating that the longer linking chain in **XW86** is favorable for improving the J_{SC}. Compared with **XW85** and **XW86**, the traditional cosensitization approach affords inferior IPCE values around the Q-band region of the porphyrin dyes within 600–750 nm, which may be related to the very small amount of adsorbed porphyrin dye **XW10** (0.42×10^{-8} mol cm^{-2} for I_3^-/I^- and 0.2×10^{-8} mol cm^{-2} for $Co^{3+/2+}$) relative to the organic dye **XL3** (23.5×10^{-8} mol cm^{-2} for I_3^-/I^- and 17.2×10^{-8} mol cm^{-2} for $Co^{3+/2+}$) (Table 1). As a result, relatively small J_{SC} values were obtained for the cosensitized devices. These results indicate that the donor-linked CC dyes **XW85** and **XW86** are indeed effective in enhancing the spectral response and the J_{SC} of the DSSCs because of their panchromatic absorption. However, the IPCE plateau and the J_{SC} for **XW85** and **XW86** are still obviously lower than those of the acceptor-linked CC dye **XW76**, despite their similar absorption spectra. As a result, **XW85** and **XW86** exhibit lowered PCE values relative to **XW76** (Table 1).

Considering that internal factors like electron injection efficiency (η_{inj}) and dye regeneration efficiency (η_{reg}) may induce the difference in the IPCE values between the two types of CC dyes,[52,53] time-resolved fluorescence spectra of the dyes adsorbed on Al_2O_3 and TiO_2 films were checked to evaluate the

Table 1 Photovoltaic parameters of DSSCs under AM1.5 illumination (power, 100 mW cm^{-2})[a]

Dyes	Electrolyte	V_{OC} [mV]	J_{SC} [mA cm^{-2}]	J^{IPCE} [mA cm^{-2}][c]	FF [%]	PCE [%]	Dye loading [$\times 10^{-8}$ mol cm^{-2}]
XW85	I_3^-/I^-	767 ± 2	17.20 ± 0.27	15.91 (8.1%)	67.92 ± 0.52	8.96 ± 0.08	12.6
XW86	I_3^-/I^-	755 ± 2	18.55 ± 0.32	16.83 (10.2%)	69.66 ± 0.59	9.76 ± 0.16	11.7
XW10 + **XL3**[b]	I_3^-/I^-	794 ± 4	16.60 ± 0.26	14.78 (12.3%)	70.40 ± 0.23	9.28 ± 0.15	0.42 (**XW10**)/23.5(**XL3**)
XL3[40]	I_3^-/I^-	810 ± 3	16.31 ± 0.16	14.84 (9.9%)	65.81 ± 0.24	8.69 ± 0.07	25.0
XW10[26]	I_3^-/I^-	711 ± 5	17.90 ± 0.04	16.08 (11.3%)	68.4 ± 0.5	8.6 ± 0.1	9.4
XW76[40]	I_3^-/I^-	765 ± 5	19.94 ± 0.18	18.28 (9.1%)	70.70 ± 0.66	10.78 ± 0.11	8.2
XW85	$[Co(bpy)_3]^{3+/2+}$	923 ± 2	11.79 ± 0.14	11.72 (0.6%)	71.65 ± 0.55	7.80 ± 0.12	7.4
XW86	$[Co(bpy)_3]^{3+/2+}$	911 ± 2	13.33 ± 0.29	13.02 (2.4%)	72.29 ± 0.80	8.78 ± 0.11	6.9
XW10 + **XL3**[b]	$[Co(bpy)_3]^{3+/2+}$	951 ± 1	11.27 ± 0.15	11.11 (1.4%)	71.59 ± 0.69	7.68 ± 0.17	0.2 (**XW10**)/17.2(**XL3**)
XL3	$[Co(bpy)_3]^{3+/2+}$	975 ± 1	10.79 ± 0.11	10.58 (2.0%)	72.10 ± 1.15	7.59 ± 0.15	17.6
XW10	$[Co(bpy)_3]^{3+/2+}$	891 ± 2	12.09 ± 0.21	11.91 (1.5%)	72.78 ± 0.49	7.84 ± 0.16	5.1
XW76	$[Co(bpy)_3]^{3+/2+}$	919 ± 2	14.63 ± 0.22	14.55 (0.5%)	72.12 ± 1.00	9.69 ± 0.13	4.2

[a] The data were collected from three parallel cells (average values and errors). [b] The TiO_2 electrode was dipped in a mixed dye solution (**XW10**/**XL3**, 1/2) in a mixture of chloroform and ethanol (1/1, v/v) for 10 h (device **M3** in the ESI). [c] The J^{IPCE} values were obtained by integrating the IPCE spectra, and the deviations from the corresponding J_{SC} values obtained from the *J–V* tests are listed in the parentheses.

electron injection dynamics. Compared to those of the dyes on Al_2O_3, the emission for all the dyes on the TiO_2 films are strongly quenched, indicating that the electrons in the excited singlet states of all the adsorbed dyes can effectively inject into TiO_2, showing high η_{inj} values exceeding 85% (Fig. S5 and Table S4, ESI†). The transient absorption measurements were further used to study the regeneration kinetics of the dyes with inert electrolyte and active redox electrolytes. The decay signals for the dye-sensitized TiO_2 films with inert electrolyte originate from the recombination between the dye cations and the injected electrons, with the recombination lifetimes (τ_{rec}) lying within 79–99 μs (Fig. S6 and Table S5, ESI†). Upon contact with the redox electrolytes, the electron transfer from the I^- or Co^{2+} species to the dye cations accelerates the decay processes, showing regeneration lifetimes of less than 10 μs and η_{reg} exceeding 90%. The relatively high η_{inj} and η_{reg} values for all the dyes ensure smooth electron injection and dye regeneration processes. Although η_{inj} and η_{reg} roughly lie in the sequence of **XW85** < **XW86** < **XW76**, identical with that of gradually improved IPCE and J_{SC}, the relatively small differences for the η_{inj} and η_{reg} values of these dyes cannot fully account for the considerable IPCE and J_{SC} differences. Another possible factor affecting IPCE and J_{SC} is the adsorption amounts of the dyes. In contrast to the fact that **XW85** and **XW86** exhibit lowered J_{SC} values relative to **XW76**, the adsorption amounts of **XW85** and **XW86** are obviously higher than that of **XW76** (Table 1). This disagreement indicates that the anchoring states for the CC dyes linked at different positions may be quite different. Hence, we continued to check their anchoring behavior.

Desorption behavior

The anchoring behavior was explored by checking the dye desorption processes. Thus, the TiO_2 films adsorbed with the dyes were soaked in 0.01 M NaOH solution (THF/H_2O), and the plots of the remaining dye percentages *versus* the soaking time are shown in Fig. 5. As a result, **XL3** and **XW10** are completely desorbed within 14 minutes, indicating that the desorption processes are rather fast for the mono-anchored dyes. In contrast, the desorption behavior of the CC dyes is considerably different. A fast desorption process in the initial 14 minutes affords 55%, 63% and 84% of the remaining adsorption amounts for **XW85**, **XW86** and **XW76**, respectively. Subsequently, a much slower desorption process was observed. When the TiO_2 films were soaked for a total of 1 h, the remaining adsorption amounts were found to be 46%, 55%, and 82%, respectively. The two desorption processes imply that the CC dyes may adsorb on the TiO_2 nanoparticles in two distinct modes, *i.e.*, single-anchoring or double-anchoring. Thus, the single-anchoring mode corresponds to the fast desorption in the first 14 minutes, while the double-anchoring relates to the subsequent slow desorption process. Judging from the desorption ratios, the acceptor-bridged CC dye **XW76** exhibits a higher ratio of double anchoring on TiO_2, compared with those of **XW85** and **XW86**. Thus, the slow desorption process for each CC dye was linearly fitted and extrapolated to evaluate the single-anchored dye amount (Fig. S7 and Table S6, ESI†). As a result, the double/single anchoring ratios were obtained to be 1.31, 1.88 and 6.34 for **XW85**, **XW86** and **XW76**, respectively. These data indicate that extending the linking chain between the donor units is favorable for enhancing the double-anchoring ratio, and the double/single anchoring ratios for the donor-linked CC dyes (**XW85** and **XW86**) are considerably lower than that for the acceptor-linked one (**XW76**). These

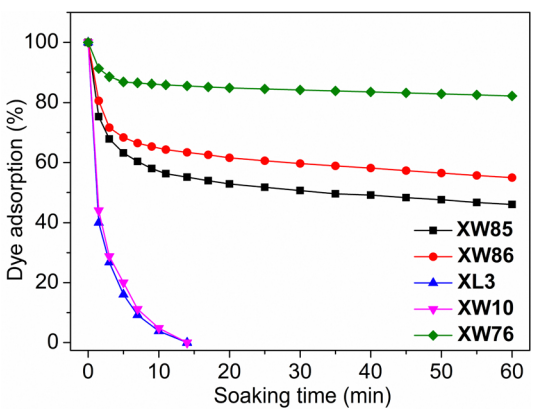

Fig. 5 Plots of the decrease in dye adsorption amounts *versus* the soaking time in 0.01 M NaOH solution (THF/H_2O, 1/1).

desorption results are consistent with the theoretical calculations (*vide infra*).

To further monitor the anchoring states of the dyes, the ATR-FTIR spectra of the dyes have been collected. All the dyes show a characteristic C=O stretching band of the carboxyl group at $\sim$1690 cm^{-1} (Fig. S8, ESI†). Upon anchoring onto the TiO_2 films, this peak disappears for **XL3**, **XW10**, and **XW76**, while the peak at $\sim$1390 cm^{-1} attributable to symmetric stretching vibrations (ν_{sym}) of COO^- is considerably intensified, indicating the nearly complete deprotonation and adsorption of the dyes on the TiO_2 surface. In contrast, the corresponding spectra for the adsorbed dyes of **XW85** and **XW86** still exhibit a weak peak at 1689 cm^{-1}, indicating the presence of considerable amounts of non-adsorbed carboxyl groups, which is consistent with the existence of mono-anchored dyes as revealed by the desorption study (*vide supra*). Similar results have also been reported for other multi-anchoring dyes.[54,55] In addition, the desorption processes for the dyes were also monitored by ATR-FTIR. Unfortunately, no obvious peak could be observed at $\sim$1690 cm^{-1} corresponding to free carboxyl groups after the initial fast desorption stage (2 min) for **XW85** and **XW86**, although the single-anchored dye has not been completely desorbed at this stage. This result may be attributed to the formation of carboxylate salts under strongly basic conditions. Further prolonged desorption time (14 and 60 min) afforded similar IR characters.

Accompanying the trend of decreasing double/single anchoring ratios, decreasing J_{SC} values were obtained for the CC dyes **XW76**, **XW86**, and **XW85**, despite the increasing adsorption amounts (Table 1). These observations indicate that each singly anchored CC dye molecule may contain a sub-dye unit hanging away from TiO_2, and thus it occupies a smaller area on the TiO_2 film. As a result, more dye molecules may be adsorbed, leading to an increase in the adsorption amounts, which may partially compensate for the J_{SC} loss induced by the single anchoring effect. In addition, the effective energy transfer from the organic dye unit to the porphyrin dye unit may also partially compensate for the J_{SC} loss. As a consequence, the lowered J_{SC} values obtained for **XW85** and **XW86** (17.20 and 18.55 mA cm^{-2}) are still comparable to that of **XW76** (19.94 mA cm^{-2}) despite the unfavorable single anchoring effect.

Theoretical calculations

To further understand the anchoring behavior of the CC dyes, theoretical calculations were performed (Fig. S9, ESI†).[56,57] The binding energies (E_{be}) were calculated by subtracting the energy of the total system from the sum of the respective energies of the dye and TiO_2: $E_{be} = (E_{dye} + E_{TiO2}) - E_{dye/TiO2}$. The calculated E_{be} values for the double-anchored dyes lie in the order of **XW85** (23.8 kcal mol^{-1}) < **XW86** (26.0 kcal mol^{-1}) < **XW76** (38.4 kcal mol^{-1}) (Table S7, ESI†), consistent with the much stronger adsorption of **XW76** than **XW85** and **XW86** revealed by the desorption study. Furthermore, the E_{be} values for the two single-anchoring modes of **XW85** and **XW86** were calculated to be much smaller, lying within the range of 1.7–11.0 kcal mol^{-1}, implying that the adsorption of the mono-anchored dyes may be weaker and easier to desorb from the film, which is fully consistent with the desorption studies (*vide supra*). As mentioned above, the porphyrin dye **XW10** adsorbs much less efficiently than the organic dye **XL3** in the cosensitized systems. However, theoretical calculations reveal that there is no obvious difference between their E_{be} values, indicating that the preferable adsorption of **XL3** in the cosensitization systems may be related to its smaller molecular size. In contrast, the single-anchored CC dyes **XW85** and **XW86** exhibit quite different adsorption behavior. The adsorption *via* the porphyrin unit may be preferable, as evidenced by the higher E_{be} values (8.9 and 11.0 kcal mol^{-1}) relative to those of adsorption *via* the organic unit (1.7 and 6.1 kcal mol^{-1}) (Table S7, ESI†). As a result, the energy transfer from the organic dye unit to the porphyrin unit may indeed partially compensate for the J_{SC} loss induced by the single anchoring of **XW85** and **XW86** (*vide supra*).

Electrochemical impedance spectroscopy

The electrochemical impedance spectroscopy (EIS) data for the DSSCs were measured in the dark to explore the effect of electrode interface properties on the V_{OC}. Theoretically, for a certain redox couple, the V_{OC} is mainly dominated by the semiconductor conduction band energy level (E_{CB}) and the free electron density,[51] and the E_{CB} for TiO_2 is affected by the density of states (DOS),[58] which is proportional to the capacitance (C_μ) level. As a result, the DSSCs based on the I_3^-/I^- electrolyte exhibit slightly different DOS values for all the dyes at a fixed bias voltage (Fig. 6a), indicative of a relatively weak effect of the conduction band shift on the V_{OC}. On the other hand, the free electron density is mainly governed by the charge recombination resistance (R_{rec}) values, which increase in the order of **XW10** (60.0 Ω cm^2) < **XW86** (81.8 Ω cm^2) < **XW76** (171.6 Ω cm^2) < **XW85** (199.9 Ω cm^2) < **XW10** + **XL3** (698.6 Ω cm^2) < **XL3** (784.1 Ω cm^2) at the fixed bias voltage of −0.75 V (Fig. 6b), in a trend the same as that of increasing V_{OC} values. On this basis, the electron lifetimes (τ) were calculated from the equation of $\tau = C_\mu \times R_{rec}$ and plotted against DOS (Fig. 6c). At the same DOS, the order of increasing τ values is roughly consistent with those of increasing R_{rec} and V_{OC} values. These results indicate that the densities of the free electrons in the TiO_2 films dominate the V_{OC} of the devices. Similar EIS properties were also observed for the cobalt-based DSSCs (Fig. S10 and Table S8, ESI†).

The similar C_μ values obtained for **XW85** and **XW86** indicate that the linking chain lengths only slightly affect the conduction band positions. On the other hand, ethylene glycol units can usually trap Li^+, shift the CB upward and thus enhance the V_{OC}.[59] However, **XW85** exhibits a C_μ close to that of **XW76**. The slightly higher V_{OC} obtained for **XW85** may be related to the fact that the adsorption amount for **XW85** is obviously higher than that of **XW76** and thus a more compact dye layer is formed for **XW85**, which suppresses the charge recombination process as thus a higher R_{rec} is observed for **XW85**. Compared with **XW86**, **XW85** possesses a shorter linkage and it shows higher R_{rec} and V_{OC} values (Table 1), indicating that the presence of a more non-anchored sub-dye unit may block the penetration of oxidized species in the electrolyte to approach TiO_2, and thus

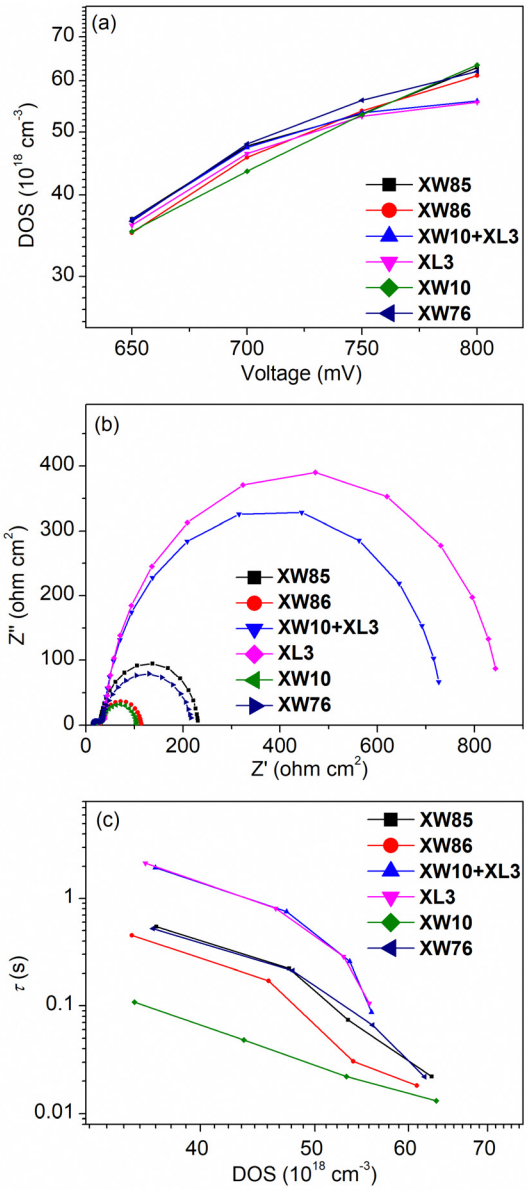

Fig. 6 (a) Plots of DOS *versus* the bias voltages, (b) complex-plane plots at applied voltage of −0.75 V, and (c) τ *versus* DOS of the DSSCs using I_3^-/I^- electrolyte measured in the dark.

suppress charge recombination. Based on the EIS data, the electron collection efficiencies (η_{col}) were also calculated, which lie in the ranges of 85.8–98.1% and 83.8–88.4% for I_3^-/I^- (V_{bias} = −0.75 V) and $Co^{3+/2+}$ (V_{bias} = −0.85 V), respectively (Table S8, ESI†). The lower η_{col} values obtained for the cobalt electrolyte are consistent with the lower J_{SC} and IPCE platforms observed for the corresponding DSSCs (Fig. 4b and d).

Durability

The PCE of the DSSCs soaked in long-term visible light was monitored to evaluate the photostability, which is a crucial factor for practical applications of DSSCs.[60] The cells sensitized by **XW85** and **XW86** with I_3^-/I^- redox shuttle provided PCEs of 8.05% and 8.86% after 500 h of visible light soaking, which are

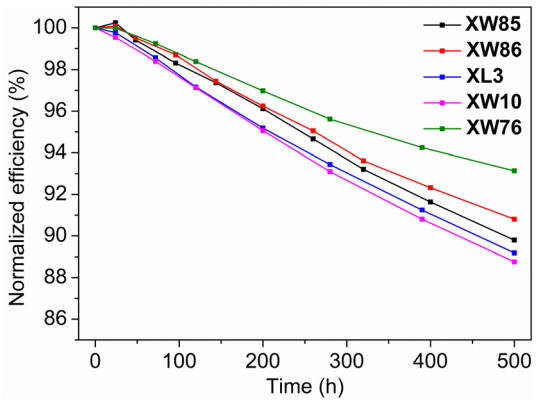

Fig. 7 Plots of the changes in the PCEs *vs.* the illumination time for the solar cells sensitized by **XW85**, **XW86**, **XL3**, **XW10** and **XW76**, respectively.

89.8% and 90.8% of the initial efficiencies, respectively (Fig. 7), lying between those of 88.8% and 93.1% observed for **XW10** and **XW76**, respectively. The sequence agrees well with that of the double/single anchoring ratios, *i.e.*, the singly anchored dye **XW10** exhibits the worst photostability. Whereas, **XW85**, **XW86** and **XW76** exhibit increasing photostability with the double/single anchoring ratios gradually improving from 1.31 to 6.34. These results indicate that enhancing the double anchoring proportion will improve the photostability, which is favorable for real applications.

Conclusions

In summary, two novel CC dyes **XW85** and **XW86** have been constructed by linking the donors of two sub-dye units corresponding to **XL3** and **XW10** with flexible chains of C_6H_{12} and $C_{12}H_{24}$, respectively. Compared to **XW85**, **XW86** exhibits higher J_{SC} values of 18.55 and 13.33 mA cm^{-2} and PCEs of 9.76% and 8.78% for I_3^-/I^- and $[Co(bpy)_3]^{3+/2+}$ electrolytes, respectively, which are also higher than those of the cosensitized DSSCs based on **XL3** and **XW10**. However, the PCE of **XW86** does not outperform that of the acceptor-linked reference CC dye **XW76**. The desorption study revealed that the CC dyes may adsorb either in the double anchoring mode or the single anchoring mode, and the double/single anchoring ratios lie in the increasing sequence of **XW85** (1.31) < **XW86** (1.88) < **XW76** (6.34), consistent with the sequence of increasing PCE. These results indicate that the lower photovoltaic performance of **XW85** and **XW86** relative to **XW76** may be related to the fact that the non-adsorbed sub-dye unit in the mono-anchored dye molecules may not effectively contribute to electron injection, and thus large portions of mono-anchoring observed for **XW85** and **XW86** result in their relatively poor J_{SC} and PCE. Compared with **XW85**, the larger double/single anchoring ratio observed for **XW86** indicates that elongation of the linking chain is favorable for double anchoring, leading to an enhanced J_{SC} of **XW86**, despite its smaller adsorption amount than that of **XW85**.

The adverse single-anchoring problem of the CC dyes revealed in this work indicates that the photovoltaic behavior may be further enhanced by addressing this problem through

more rational molecular design in the future. For example, both the donors and the acceptors of the respective sub-dye units may be linked with flexible chains to rule out the possibility of opposite alignment of the two carboxyl groups between sub-dye units and thus simultaneously anchor the carboxyl groups, resulting in enhanced J_{SC} and PCE.

Experimental

Synthesis of the CC dyes XW85–XW86

Compounds **PTZ-a**, **PTZ-b**, **BT-BTD-A**, and **ZnP-A** were synthesized according to the literature.[47–49] The synthetic routes for dyes **XW85** and **XW86** are shown in Scheme 1 with the details described as follows:

1a. To the mixture of **PTZ-a** (440 mg, 0.55 mmol) and (4-(hexyloxy)phenyl)boronic acid (307 mg, 1.38 mmol) in THF (20 mL) were added 2 M K_2CO_3 aqueous solution (1.40 mL, 2.80 mmol) and $Pd(PPh_3)_4$ (32 mg, 0.03 mmol) under a nitrogen atmosphere. The mixture was refluxed for 18 h, and then a saturated aqueous solution of ammonium chloride was added at room temperature. The mixture was extracted with dichloromethane (DCM) (50 mL × 3) and the organic phase was dried over Na_2SO_4, filtered, and then concentrated under reduced pressure. The obtained residue was purified by silica gel column chromatography with DCM/petroleum ether (1/6, v/v) as the eluent to give a yellow solid of **1a** (100 mg, 19%). ^{1}H NMR (400 MHz, $CDCl_3$, ppm): δ 7.41 (d, J = 8.5 Hz, 4H), 7.30 (d, J = 8.7 Hz, 2H), 7.27 (s, 2H), 7.23–7.19 (m, 4H), 6.95–6.90 (m, 4H), 6.83 (d, J = 8.4 Hz, 2H), 6.66 (d, J = 8.4 Hz, 2H), 3.98 (t, J = 6.6 Hz, 4H), 3.80 (s, 4H), 1.84–1.74 (m, 8H), 1.51–1.42 (m, 8H), 1.38–1.32 (m, 8H), 0.95–0.87 (m, 6H). ^{13}C NMR (151 MHz, $CDCl_3$): δ 158.54, 144.32, 143.40, 135.57, 132.06, 129.84, 129.65, 127.44, 126.99, 125.57, 125.43, 124.59, 116.45, 115.68, 114.76, 114.35, 68.05, 47.09, 31.57, 29.23, 26.44, 26.25, 25.71, 22.59, 14.03. HRMS (ESI, m/z): $[M + H]^+$ calcd for $C_{54}H_{59}Br_2N_2O_2S_2$, 989.2385; found, 989.2382. FT-IR (ATR, cm^{-1}): 2931 (m), 2855 (m), 1604 (m), 1580 (w), 1518 (w), 1491 (m), 1458 (s), 1393 (s), 1375 (m), 1234 (s), 1187 (m), 1107 (m), 1023 (m), 876 (m), 798 (s), 749 (m), 679 (w), 606 (m). mp 119–121 °C.

1b. The synthetic procedure resembles that for synthesizing compound **1a** except using compound **PTZ-b** (2.88 g, 3.27 mmol) instead of **PTZ-a**. The obtained crude product was purified by silica gel column chromatography with DCM/petroleum ether (1/6, v/v) as the eluent to give a yellow viscous liquid of **1b** (600 mg, 17%). ^{1}H NMR (400 MHz, $CDCl_3$, ppm): δ 7.42 (d, J = 8.5 Hz, 4H), 7.35–7.28 (m, 4H), 7.25–7.18 (m, 4H), 6.95–6.91 (m, 4H), 6.86 (d, J = 8.4 Hz, 2H), 6.69 (d, J = 8.5 Hz, 2H), 3.97 (t, J = 6.6 Hz, 4H), 3.80 (s, 4H), 1.84–1.73 (m, 8H), 1.50–1.38 (m, 8H), 1.37–1.31 (m, 8H), 1.29–1.18 (m, 12H), 0.94–0.88 (m, 6H). ^{13}C NMR (151 MHz, $CDCl_3$): δ 158.55, 144.32, 143.43, 135.49, 132.11, 129.83, 129.57, 127.43, 126.77, 125.58, 125.37, 124.35, 116.39, 115.61, 114.78, 114.27, 68.07, 47.47, 31.62, 29.48, 29.41, 29.27, 29.17, 26.82, 26.67, 25.75, 22.63, 14.10, 14.08. HRMS (ESI, m/z): $[M + H]^+$ calcd for $C_{60}H_{71}Br_2N_2O_2S_2$, 1073.3324, found, 1073.3317. FT-IR (ATR, cm^{-1}): 2931 (m), 2855 (m), 1605 (m), 1580 (w), 1518 (w), 1491 (m), 1458 (s), 1393 (s), 1375 (m), 1235 (s), 1186 (m), 1107 (m), 1023 (m), 876 (m), 798 (s), 749 (m), 678 (w), 606 (m).

2a. To the mixture of $Pd_2(dba)_3$ (6 mg, 0.01 mmol), $AsPh_3$ (34 mg, 0.11 mmol), compound **1a** (110 mg, 0.11 mmol), and **ZnP-A** (80 mg, 0.06 mmol) in THF (12 mL) was added triethylamine (3 mL) under a nitrogen atmosphere. The solution was refluxed for 18 h. After cooling down to room temperature, the reaction mixture was concentrated under reduced pressure. The obtained residue was purified by silica gel column chromatography with DCM/petroleum ether (2/3, v/v) as the eluent to give a dark green solid of **2a** (90 mg, 69%). ^{1}H NMR (400 MHz, $CDCl_3$, ppm): δ 9.63 (d, J = 4.6 Hz, 2H), 9.59 (d, J = 4.5 Hz, 2H), 8.88 (d, J = 4.6 Hz, 2H), 8.84 (d, J = 4.5 Hz, 2H), 8.18–8.14 (m, 2H), 8.01–7.97 (m, 2H), 7.77–7.68 (m, 4H), 7.48–7.44 (m, 2H), 7.38–7.29 (m, 3H), 7.25–7.20 (m, 5H), 7.02 (d, J = 8.4 Hz, 4H), 6.99–6.89 (m, 4H), 6.82 (d, J = 8.5 Hz, 1H), 6.69 (d, J = 9.3 Hz, 1H), 6.43 (d, J = 8.7 Hz, 2H), 4.01–3.94 (m, 7H), 3.90–3.78 (m, 10H), 3.37 (t, J = 6.6 Hz, 2H), 1.93–1.75 (m, 6H), 1.39–1.32 (m, 6H), 1.30–1.23 (m, 16H), 1.19–1.10 (m, 10H), 1.09–0.83 (m, 52H), 0.70–0.59 (m, 8H), 0.58–0.39 (m, 24H). ^{13}C NMR (151 MHz, $CDCl_3$): δ 166.67, 159.93, 158.49, 158.11, 151.65, 151.34, 150.60, 150.48, 144.34, 143.40, 139.60, 135.59, 133.70, 132.15, 132.06, 131.95, 131.63, 131.06, 130.53, 130.17, 129.87, 129.77, 129.69, 129.64, 128.64, 128.44, 127.43, 127.26, 125.66, 125.50, 125.45, 125.41, 124.68, 124.44, 123.98, 123.27, 122.46, 121.91, 121.54, 120.94, 116.45, 115.73, 115.63, 115.31, 115.27, 114.78, 114.75, 114.35, 105.10, 68.58, 68.06, 67.97, 67.92, 64.80, 47.24, 47.15, 31.84, 31.61, 31.53, 31.50, 30.21, 30.15, 30.13, 29.95, 29.90, 29.87, 29.87, 29.83, 29.80, 29.49, 29.40, 29.29, 29.25, 29.14, 29.09, 28.98, 28.76, 28.65, 26.54, 26.45, 26.35, 26.28, 26.20, 25.73, 25.57, 25.27, 23.27, 22.64, 22.62, 22.56, 16.11, 14.09, 14.06, 14.03. HRMS (ESI, m/z): $[M + H]^+$ calcd for $C_{146}H_{180}BrN_6O_8S_2Zn$, 2352.1779, found, 2352.1724. FT-IR (ATR, cm^{-1}): 2920 (s), 2850 (s), 2187 (m), 1720 (m), 1602 (m), 1586 (m), 1518 (w), 1492 (m), 1457 (s), 1392 (m), 1237 (s), 1206 (m), 1099 (s), 995 (m), 876 (w), 795 (m), 714 (m). mp 78–80 °C.

2b. The synthetic procedure resembles that for synthesizing compound **2a** except using compound **1b** (200 mg, 0.19 mmol) instead of **1a**. The obtained crude product was purified by silica gel column chromatography with DCM/petroleum ether (2/3, v/v) as the eluent to give a dark green solid of **2b** (90 mg, 59%). ^{1}H NMR (400 MHz, $CDCl_3$, ppm): δ 9.62 (d, J = 4.6 Hz, 4H), 8.89 (d, J = 4.6 Hz, 2H), 8.86 (d, J = 4.6 Hz, 2H), 8.17–8.08 (m, 2H), 7.95 (t, J = 6.2 Hz, 2H), 7.78–7.67 (m, 4H), 7.47 (d, J = 8.7 Hz, 2H), 7.40–7.31 (m, 4H), 7.25–7.16 (m, 4H), 7.02 (d, J = 8.5 Hz, 4H), 6.98 (d, J = 8.4 Hz, 1H), 6.94 (dd, J = 8.6, 2.7 Hz, 3H), 6.81 (dd, J = 8.8, 5.5 Hz, 3H), 6.66 (d, J = 8.5 Hz, 1H), 4.01–3.91 (m, 7H), 3.87 (t, J = 6.5 Hz, 10H), 3.78 (t, J = 7.1 Hz, 2H), 1.96–1.86 (m, 2H), 1.82–1.67 (m, 6H), 1.39–1.21 (m, 22H), 1.21–1.10 (m, 8H), 1.09–0.94 (m, 32H), 0.95–0.83 (m, 12H), 0.83–0.74 (m, 20H), 0.68–0.58 (m, 8H), 0.56–0.36 (m, 24H). ^{13}C NMR (151 MHz, $CDCl_3$): δ 166.36, 159.95, 158.36, 158.25, 151.73, 151.41, 150.63, 150.51, 145.01, 144.31, 143.40, 143.18, 135.47, 135.34, 132.15, 132.05, 131.92, 131.76, 130.74, 130.68, 130.00, 129.96, 129.88, 129.81, 129.55, 129.31, 127.32, 127.19, 126.78,

125.48, 125.34, 125.25, 124.46, 124.37, 124.27, 124.24, 120.83, 116.37, 115.58, 115.54, 115.50, 114.77, 114.68, 114.23, 114.20, 105.16, 68.65, 68.06, 68.00, 47.71, 47.46, 31.86, 31.62, 31.60, 29.56, 29.49, 29.40, 29.29, 29.27, 29.21, 29.15, 29.09, 28.77, 28.67, 26.95, 26.85, 26.82, 26.68, 26.64, 25.73, 25.69, 25.33, 22.66, 22.64, 22.61, 14.12, 14.07. HRMS (ESI, *m*/*z*): $[M + H]^+$ calcd for $C_{152}H_{192}BrN_6O_8S_2Zn$, 2436.2718, found, 2436.2712. FT-IR (ATR, cm^{-1}): 2920 (s), 2849 (s), 2187 (m), 1719 (m), 1602 (m), 1586 (m), 1518 (w), 1495 (w), 1456 (s), 1391 (m), 1240 (s), 1206 (m), 1096 (s), 996 (m), 879 (w), 791 (m), 712 (m). mp 66–68 °C.

3a. To the mixture of compound **2a** (71 mg, 0.03 mmol), bis(pinacolato)diboron (9 mg, 0.04 mmol), and KOAc (15 mg, 0.15 mmol) in 1,4-dioxane (10 mL) was added $Pd(PPh_3)_2Cl_2$ (5 mg, 0.01 mmol) under a nitrogen atmosphere. The mixture was refluxed for 18 h, and then a saturated aqueous solution of ammonium chloride was added to the reaction mixture at room temperature. The mixture was extracted with DCM (50 mL × 3) and the organic phase was dried over Na_2SO_4, filtered, and then concentrated under reduced pressure. The obtained residue was purified by flash silica gel column chromatography with DCM/petroleum ether (2/1, v/v) as the eluent. The obtained green residue was used for the next reaction without further characterization. To the mixture of the obtained residue and **BT-BTD-A** (24 mg, 0.03 mmol) in THF (10 mL) were added 2 M K_2CO_3 aqueous solution (0.10 mL, 0.20 mmol) and $Pd(PPh_3)_4$ (3 mg, 0.003 mmol) under a nitrogen atmosphere. The reaction was refluxed for 18 h, and then a saturated aqueous solution of ammonium chloride was added to the reaction mixture at room temperature. The mixture was extracted with DCM (50 mL × 3) and the organic phase was dried over Na_2SO_4, filtered, and then concentrated under reduced pressure. The obtained residue was purified by silica gel column chromatography with DCM/petroleum ether (3/2, v/v) as the eluent to give a brown solid of **3a** (25 mg, 29% (two steps)). ^{1}H NMR (400 MHz, $CDCl_3$, ppm): δ 9.57 (d, J = 4.5 Hz, 2H), 9.51 (d, J = 4.6 Hz, 2H), 8.85 (d, J = 4.6 Hz, 2H), 8.80 (d, J = 4.5 Hz, 2H), 8.14 (d, J = 8.3 Hz, 2H), 8.00 (d, J = 8.3 Hz, 2H), 7.97 (d, J = 8.3 Hz, 2H), 7.74 (d, J = 8.5 Hz, 2H), 7.70 (d, J = 6.4 Hz, 2H), 7.55–7.50 (m, 3H), 7.48–7.43 (m, 2H), 7.40–7.36 (m, 4H), 7.34–7.28 (m, 4H), 7.23 (d, J = 2.1 Hz, 1H), 7.04 (d, J = 8.6 Hz, 5H), 6.97–6.91 (m, 5H), 6.87 (dd, J = 8.5, 6.9 Hz, 2H), 6.61 (d, J = 8.6 Hz, 2H), 3.99–3.94 (m, 12H), 3.90 (t, J = 6.6 Hz, 8H), 3.58 (t, J = 6.6 Hz, 2H), 2.64 (t, J = 7.9 Hz, 4H), 1.95–1.75 (m, 8H), 1.63 (s, 8H), 1.38–1.22 (m, 28H), 1.19–1.11 (m, 8H), 1.09–0.98 (m, 20H), 0.96–0.86 (m, 24H), 0.84–0.75 (m, 20H), 0.72–0.65 (m, 8H), 0.61–0.48 (m, 20H). ^{13}C NMR (151 MHz, $CDCl_3$): δ 166.68, 166.55, 159.87, 158.49, 151.63, 151.28, 150.47, 150.39, 149.20, 144.92, 143.48, 143.20, 139.33, 139.30, 138.64, 136.04, 135.61, 135.46, 132.28, 132.17, 131.88, 131.57, 131.12, 130.96, 130.87, 130.55, 130.25, 130.13, 130.03, 130.00, 129.96, 129.87, 129.84, 129.79, 129.65, 129.53, 129.48, 129.37, 129.01, 128.79, 128.70, 128.16, 127.72, 127.59, 127.43, 127.25, 125.58, 125.51, 125.43, 125.11, 124.68, 124.64, 124.59, 124.52, 123.87, 120.79, 118.52, 118.31, 115.70, 115.45, 115.33, 115.22, 115.09, 114.79, 114.74, 105.13, 68.65, 68.04, 68.03, 47.23, 31.78, 31.68, 31.62, 31.56, 31.48, 30.89, 30.27, 30.19, 29.82, 29.76, 29.74, 29.66, 29.52, 29.48, 29.44, 29.42, 29.32, 29.28, 29.21, 29.18, 29.16, 29.13, 29.08, 29.06, 29.01, 28.99, 28.97, 28.95, 28.92, 28.72, 28.63, 27.16, 27.14, 26.23, 26.16, 26.07, 25.70, 25.51, 25.27, 22.65, 22.60, 22.58, 22.53, 14.14, 14.10, 14.08, 14.04, 13.99. MS (MALDI-TOF, *m*/*z*): $[M]^+$ calcd for $C_{182}H_{216}N_8O_{10}S_5Zn$, 2897.5; found, 2897.2. FT-IR (ATR, cm^{-1}): 2919 (s), 2849 (s), 2188 (m), 1720 (s), 1601 (s), 1586 (s), 1498 (w), 1455 (s), 1392 (m), 1270 (s), 1240 (s), 1205 (m), 1097 (s), 996 (m), 878 (w), 792 (m), 766 (m), 713 (m). mp 85–87 °C.

3b. The synthetic procedure resembles that for synthesizing compound **3a** except using compound **2b** (70 mg, 0.03 mmol) instead of **2a**. The obtained crude product was purified by silica gel column chromatography with DCM/petroleum ether (3/2, v/v) as the eluent to give a brown solid of **3b** (25 mg, 29% (two steps)). ^{1}H NMR (400 MHz, $CDCl_3$, ppm): δ 9.62–9.57 (m, 4H), 8.87 (d, J = 4.6 Hz, 2H), 8.84 (d, J = 4.5 Hz, 2H), 8.15 (d, J = 7.6 Hz, 2H), 7.97 (d, J = 8.2 Hz, 2H), 7.91 (s, 1H), 7.88 (d, J = 4.9 Hz, 2H), 7.76 (s, 1H), 7.73 (d, J = 8.3 Hz, 2H), 7.69 (d, J = 2.4 Hz, 2H), 7.62 (s, 2H), 7.46 (d, J = 8.7 Hz, 2H), 7.42 (d, J = 8.4 Hz, 2H), 7.38 (d, J = 8.7 Hz, 2H), 7.38–7.31 (m, 2H), 7.31 (d, J = 2.1 Hz, 1H), 7.30–7.27 (m, 3H), 7.02 (d, J = 8.5 Hz, 4H), 6.93 (d, J = 8.5 Hz, 4H), 6.90–6.86 (m, 2H), 6.84 (d, J = 8.8 Hz, 2H), 3.98 (d, J = 2.0 Hz, 3H), 3.96 (d, J = 6.6 Hz, 2H), 3.91 (s, 5H), 3.90–3.83 (m, 12H), 2.73 (t, J = 7.7 Hz, 2H), 2.67 (t, J = 7.9 Hz, 2H), 1.93–1.82 (m, 4H), 1.81–1.61 (m, 8H), 1.45–1.39 (m, 4H), 1.38–1.31 (m, 20H), 1.30–1.23 (m, 16H), 1.19–1.11 (m, 8H), 1.08–0.96 (m, 22H), 0.94–0.85 (m, 22H), 0.84–0.77 (m, 20H), 0.68–0.60 (m, 8H), 0.59–0.47 (m, 16H), 0.46–0.38 (m, 8H). ^{13}C NMR (151 MHz, $CDCl_3$): δ 166.67, 166.42, 159.91, 159.87, 158.47, 158.35, 152.18, 151.66, 151.36, 150.56, 150.44, 149.45, 144.95, 144.49, 143.39, 143.14, 139.85, 139.51, 138.92, 136.40, 135.47, 135.30, 132.19, 132.15, 131.99, 131.66, 131.06, 130.94, 130.81, 130.78, 130.62, 130.41, 130.26, 129.94, 129.81, 129.64, 129.52, 129.38, 129.27, 129.00, 128.81, 128.45, 128.12, 128.01, 127.84, 127.71, 127.40, 127.31, 126.03, 125.46, 125.42, 125.40, 125.34, 124.63, 124.54, 124.51, 124.36, 124.32, 120.80, 118.77, 118.11, 115.53, 115.45, 115.39, 115.01, 114.97, 114.75, 114.70, 105.16, 101.26, 98.79, 68.62, 68.05, 68.02, 67.98, 47.66, 47.46, 32.03, 31.80, 31.66, 31.62, 31.58, 31.55, 31.47, 31.40, 31.01, 30.97, 30.92, 30.42, 30.36, 30.31, 30.28, 30.22, 30.15, 30.10, 30.03, 29.99, 29.90, 29.89, 29.85, 29.76, 29.74, 29.68, 29.50, 29.43, 29.36, 29.33, 29.31, 29.29, 29.24, 29.21, 29.17, 29.15, 29.07, 29.00, 28.99, 28.70, 28.60, 27.64, 27.18, 27.12, 27.09, 26.90, 26.78, 26.76, 26.68, 26.65, 26.62, 26.56, 26.52, 26.47, 25.71, 25.67, 25.25, 22.64, 22.60, 22.57, 14.12, 14.10, 14.06, 14.01. MS (MALDI-TOF, *m*/*z*): $[M]^+$ calcd for $C_{188}H_{228}N_8O_{10}S_5Zn$, 2981.5; found, 2981.4. FT-IR (ATR, cm^{-1}): 2919 (s), 2849 (s), 2188 (m), 1720 (s), 1600 (s), 1586 (s), 1498 (w), 1454 (s), 1392 (m), 1269 (s), 1240 (s), 1205 (m), 1096 (s), 996 (m), 878 (w), 792 (m), 765 (m), 713 (m). mp 76–78 °C.

XW85. Compound **3a** (25 mg, 0.01 mmol) and $LiOH{\cdot}H_2O$ (56 mg, 1.3 mmol) were mixed in a solvent of THF/H_2O (10 mL, 4/1, v/v). The mixture was refluxed for 24 h and then cooled down to room temperature. The reaction mixture was acidified with 2 M HCl to pH = 1–3 and extracted with DCM (50 mL × 3). The organic phase was dried over Na_2SO_4, filtered, and then concentrated under reduced pressure. The crude product was

purified by silica gel column chromatography with DCM/methanol (30/1, v/v) as the eluent to give a brown solid of **XW85** (22 mg, 89%). ^{1}H NMR (400 MHz, DMSO-d_6: $CDCl_3$ = 2 : 1(v: v), ppm): δ 9.56 – 9.49 (m, 4H), 8.72 (d, J = 4.6 Hz, 2H), 8.69 (d, J = 4.5 Hz, 2H), 8.17 (s, 2H), 8.15 (s, 2H), 8.05 (d, J = 8.4 Hz, 2H), 8.01–7.97 (m, 3H), 7.92 (s, 1H), 7.85 (d, J = 8.0 Hz, 1H), 7.79 (d, J = 7.7 Hz, 1H), 7.76 (d, J = 8.8 Hz, 1H), 7.71–7.66 (m, 2H), 7.66 (d, J = 1.8 Hz, 1H), 7.57 (d, J = 8.2 Hz, 2H), 7.44 (d, J = 8.4 Hz, 2H), 7.37 (d, J = 8.5 Hz, 2H), 7.33 (d, J = 8.1 Hz, 1H), 7.30–7.27 (m, 2H), 7.24 (d, J = 8.0 Hz, 1H), 7.21 (d, J = 1.8 Hz, 1H), 7.03 (d, J = 8.5 Hz, 4H), 6.94 (d, J = 8.5 Hz, 2H), 6.90–6.85 (m, 3H), 6.81 (d, J = 8.5 Hz, 2H), 3.91 (t, J = 6.5 Hz, 4H), 3.83 (t, J = 6.6 Hz, 12H), 2.80–2.75 (m, 2H), 2.71 (t, J = 1.9 Hz, 2H), 1.74–1.64 (m, 8H), 1.44–1.39 (m, 8H), 1.33–1.27 (m, 18H), 1.23–1.18 (m, 12H), 1.16–1.09 (m, 8H), 1.07–1.00 (m, 16H), 0.97–0.91 (m, 14H), 0.90–0.82 (m, 20H), 0.79–0.72 (m, 18H), 0.59–0.50 (m, 14H), 0.40–0.31 (m, 8H). MS (MALDI-TOF, m/z): $[M]^+$ calcd for $C_{180}H_{212}N_8O_{10}S_5Zn$, 2869.4; found, 2869.3. FT-IR (ATR, cm^{-1}): 2920 (s), 2848 (s), 2187 (m), 1689 (s), 1585 (s), 1500 (w), 1454 (s), 1390 (m), 1242 (s), 1205 (m), 1095 (s), 997 (m), 879 (w), 791 (m), 768 (m), 710 (m). mp 121–123 °C.

XW86. The synthetic procedure resembles that for synthesizing compound **XW85** except using compound **3b** (25 mg, 0.01 mmol) instead of **3a**. The crude product was purified by silica gel column chromatography with DCM/methanol (30/1, v/v) as the eluent to give a brown solid of **XW86** (21 mg, 85%). ^{1}H NMR (400 MHz, DMSO-d_6: $CDCl_3$ = 2 : 1 (v: v), ppm): δ 9.56–9.49 (m, 4H), 8.72 (d, J = 4.7 Hz, 2H), 8.69 (d, J = 4.5 Hz, 2H), 8.16 (s, 2H), 8.15 (s, 2H), 8.05 (d, J = 8.4 Hz, 2H), 8.02–7.96 (m, 3H), 7.91 (s, 1H), 7.85 (d, J = 8.3 Hz, 1H), 7.79 (d, J = 7.5 Hz, 1H), 7.75 (d, J = 8.6 Hz, 1H), 7.71–7.66 (m, 2H), 7.66 (d, J = 1.7 Hz, 1H), 7.58 (d, J = 8.1 Hz, 2H), 7.43 (d, J = 8.3 Hz, 2H), 7.37 (d, J = 8.4 Hz, 2H), 7.33 (d, J = 8.8 Hz, 1H), 7.30–7.26 (m, 2H), 7.24 (d, J = 8.4 Hz, 1H), 7.21 (s, 1H), 7.03 (d, J = 8.5 Hz, 4H), 6.94 (d, J = 8.3 Hz, 2H), 6.88 (d, J = 7.7 Hz, 3H), 6.81 (d, J = 8.4 Hz, 2H), 3.91 (t, J = 6.5 Hz, 4H), 3.84 (t, J = 6.5 Hz, 12H), 2.80–2.75 (m, 2H), 2.68–2.62 (m, 2H), 1.77–1.60 (m, 12H), 1.45–1.38 (m, 8H), 1.35–1.29 (m, 18H), 1.27–1.23 (m, 24H), 1.16–1.10 (m, 8H), 1.08–1.00 (m, 12H), 0.96–0.82 (m, 36H), 0.79–0.72 (m, 16H), 0.59–0.49 (m, 14H), 0.41–0.29 (m, 8H). MS (MALDI-TOF, m/z): $[M]^+$ calcd for $C_{186}H_{224}N_8O_{10}S_5Zn$, 2953.5; found, 2953.4. FT-IR (ATR, cm^{-1}): 2920 (s), 2848 (s), 2185 (m), 1689 (s), 1600 (s), 1585 (s), 1497 (w), 1456 (s), 1392 (m), 1240 (s), 1203 (m), 1095 (s), 995 (m), 878 (w), 791 (m), 768 (m), 714 (m). mp 108–110 °C.

Further details about characterization figures, fabrication of DSSCs, and photovoltaic behavior measurements can be found in the ESI.†

Author contributions

Jiaxin Luo: formal analysis, investigation, methodology, visualization, and writing – original draft. Yuqing Wang and Glib Baryshnikov: formal analysis. Shaojin Shi, Yuankun Wu, Taochun Ma, and Leyao Wang: investigation. Xinyan Wu, Chengjie Li and Yongshu Xie: conceptualization, formal analysis, investigation, methodology, visualization, writing – review & editing, funding acquisition, and supervision.

Conflicts of interest

There are no conflicts to declare.

Acknowledgements

This work was financially supported by the National Natural Science Foundation of China (No. 22131005, 21971063, 22201074, and 22075077), the Program of Shanghai Academic Research Leader (No. 20XD1401400), the Natural Science Foundation of Shanghai (No. 20ZR1414100, 22ZR1416100), and the Fundamental Research Funds for the Central Universities (No. 222201717003).

Notes and references

1 N. Yan, C. Zhao, S. You, Y. Zhang and W. Li, *Chin. Chem. Lett.*, 2020, **31**, 643–653.
2 B. O'Regan and M. Grätzel, *Nature*, 1991, **353**, 737–740.
3 A. Yella, H.-W. Lee, H. N. Tsao, C. Yi, A. K. Chandiran, M. K. Nazeeruddin, E. W.-G. Diau, C.-Y. Yeh, S. M. Zakeeruddin and M. Grätzel, *Science*, 2011, **334**, 629–634.
4 S. Mathew, A. Yella, P. Gao, R. Humphry-Baker, B. F. E. Curchod, N. Ashari-Astani, I. Tavernelli, U. Rothlisberger, M. K. Nazeeruddin and M. Grätzel, *Nat. Chem.*, 2014, **6**, 242–247.
5 Y. Ren, D. Zhang, J. Suo, Y. Cao, F. T. Eickemeyer, N. Vlachopoulos, S. M. Zakeeruddin, A. Hagfeldt and M. Grätzel, *Nature*, 2023, **613**, 60–65.
6 Q. Yu, Y. Wang, Z. Yi, N. Zu, J. Zhang, M. Zhang and P. Wang, *ACS Nano*, 2010, **4**, 6032–6038.
7 C. E. Housecroft and E. C. Constable, *Chem. Sci.*, 2022, **13**, 1225–1262.
8 H. Jiang, Y. Ren, W. Zhang, Y. Wu, E. C. Socie, B. I. Carlsen, J.-E. Moser, H. Tian, S. M. Zakeeruddin, W.-H. Zhu and M. Grätzel, *Angew. Chem., Int. Ed.*, 2020, **59**, 9324–9329.
9 C. Liao, K. Zeng, H. Wu, Q. Zeng, H. Tang, L. Wang, H. Meier, Y. Xie and D. Cao, *Cell Rep. Phys. Sci.*, 2021, **2**, 100326.
10 D. Zhang, M. Stojanovic, Y. Ren, Y. Cao, F. T. Eickemeyer, E. Socie, N. Vlachopoulos, J.-E. Moser, S. M. Zakeeruddin, A. Hagfeldt and M. Grätzel, *Nat. Commun.*, 2021, **12**, 1777.
11 L. Zhang, X. Yang, W. Wang, G. G. Gurzadyan, J. Li, X. Li, J. An, Z. Yu, H. Wang, B. Cai, A. Hagfeldt and L. Sun, *ACS Energy Lett.*, 2019, **4**, 943–951.
12 Y. K. Eom, I. T. Choi, S. H. Kang, J. Lee, J. Kim, M. J. Ju and H. K. Kim, *Adv. Energy Mater.*, 2015, **5**, 1500300.
13 Z. Chai, J. Wang, Y. Xie, P. Lin, H. Li, K. Chang, T. Xu, A. Mei, Q. Peng, M. Wang, H. Han, Q. Li and Z. Li, *ACS Appl. Mater. Interfaces*, 2019, **11**, 27648–27657.

14 Z. Chai, M. Wu, M. Fang, S. Wan, T. Xu, R. Tang, Y. Xie, A. Mei, H. Han, Q. Li and Z. Li, *Adv. Energy Mater.*, 2015, **5**, 1500846.
15 K. Zeng, Y. Chen, W.-H. Zhu, H. Tian and Y. Xie, *J. Am. Chem. Soc.*, 2020, **142**, 5154–5161.
16 K. Zeng, Y. Lu, W. Tang, S. Zhao, Q. Liu, W. Zhu, H. Tian and Y. Xie, *Chem. Sci.*, 2019, **10**, 2186–2192.
17 S. H. Kang, M. J. Jeong, Y. K. Eom, I. T. Choi, S. M. Kwon, Y. Yoo, J. Kim, J. Kwon, J. H. Park and H. K. Kim, *Adv. Energy Mater.*, 2017, **7**, 1602117.
18 Y. Kurumisawa, T. Higashino, S. Nimura, Y. Tsuji, H. Iiyama and H. Imahori, *J. Am. Chem. Soc.*, 2019, **141**, 9910–9919.
19 T. Higashino, Y. Kurumisawa, A. B. Alemayehu, R. F. Einrem, D. Sahu, D. Packwood, K. Kato, A. Yamakata, A. Ghosh and H. Imahori, *ACS Appl. Energy Mater.*, 2020, **3**, 12460–12467.
20 Y. Hu, A. Alsaleh, O. Trinh, F. D'Souza and H. Wang, *J. Mater. Chem. A*, 2021, **9**, 27692–27700.
21 Y. Hu, W. A. Webre, M. B. Thomas, A. Moss, S. N. Hancock, J. Schaffner, F. D'Souza and H. Wang, *J. Mater. Chem. A*, 2019, **7**, 10712–10722.
22 H. Song, Q. Liu and Y. Xie, *Chem. Commun.*, 2018, **54**, 1811–1824.
23 K. Zeng, Z. Tong, L. Ma, W.-H. Zhu, W. Wu and Y. Xie, *Energy Environ. Sci.*, 2020, **13**, 1617–1657.
24 T. Higashino and H. Imahori, *ACS Energy Lett.*, 2022, **7**, 1926–1938.
25 M. Aftabuzzaman, S. Sarker, C. Lu and H. K. Kim, *J. Mater. Chem. A*, 2021, **9**, 24830–24848.
26 Y. Xie, Y. Tang, W. Wu, Y. Wang, J. Liu, X. Li, H. Tian and W.-H. Zhu, *J. Am. Chem. Soc.*, 2015, **137**, 14055–14058.
27 J.-M. Ji, H. Zhou, Y. K. Eom, C. H. Kim and H. K. Kim, *Adv. Energy Mater.*, 2020, **10**, 2000124.
28 A. Mahmood, J.-Y. Hu, B. Xiao, A. Tang, X. Wang and E. Zhou, *J. Mater. Chem. A*, 2018, **6**, 16769–16797.
29 C.-C. Chen, J.-S. Chen, V. S. Nguyen, T.-C. Wei and C.-Y. Yeh, *Angew. Chem., Int. Ed.*, 2021, **60**, 4886–4893.
30 H. Song, J. Zhang, J. Jin, H. Wang and Y. Xie, *J. Mater. Chem. C*, 2018, **6**, 3927–3936.
31 Y. Zhang, K. Ren, L. Wang, L. Wang and Z. Fan, *Chin. Chem. Lett.*, 2022, **33**, 33–60.
32 Y. Tang, X. Liu, Y. Wang, Q. Liu, X. Li, C. Li, X. Shen and Y. Xie, *Chin. Chem. Lett.*, 2020, **31**, 1927–1930.
33 C.-L. Wang, J.-Y. Hu, C.-H. Wu, H.-H. Kuo, Y.-C. Chang, Z.-J. Lan, H.-P. Wu, E. Wei-Guang Diau and C.-Y. Lin, *Energy Environ. Sci.*, 2014, **7**, 1392–1396.
34 S. Chang, H. Wang, Y. Hua, Q. Li, X. Xiao, W.-K. Wong, W. Y. Wong, X. Zhu and T. Chen, *J. Mater. Chem. A*, 2013, **1**, 11553–11558.
35 T. Hua, K. Zhang, Z.-S. Huang, L. Wang, H. Tang, H. Meier and D. Cao, *J. Mater. Chem. C*, 2019, **7**, 10379–10388.
36 J. M. Cole, G. Pepe, O. K. Al Bahri and C. B. Cooper, *Chem. Rev.*, 2019, **119**, 7279–7327.
37 Y. Lu, Q. Liu, J. Luo, B. Wang, T. Feng, X. Zhou, X. Liu and Y. Xie, *ChemSusChem*, 2019, **12**, 2802–2809.
38 J. Zou, Y. Tang, G. Baryshnikov, Z. Yang, R. Mao, W. Feng, J. Guan, C. Li and Y. Xie, *J. Mater. Chem. A*, 2022, **10**, 1320–1328.
39 Y. Chen, Y. Tang, J. Zou, K. Zeng, G. Baryshnikov, C. Li and Y. Xie, *ACS Appl. Mater. Interfaces*, 2021, **13**, 49828–49839.
40 J. Luo, Z. Xie, J. Zou, X. Wu, X. Gong, C. Li and Y. Xie, *Chin. Chem. Lett.*, 2022, **33**, 4313–4316.
41 J. Zou, Y. Wang, G. Baryshnikov, J. Luo, X. Wang, H. Ågren, C. Li and Y. Xie, *ACS Appl. Mater. Interfaces*, 2022, **14**, 33274–33284.
42 S. Jiang, S. Fan, X. Lu, G. Zhou and Z.-S. Wang, *J. Mater. Chem. A*, 2014, **2**, 17153–17164.
43 Z.-S. Huang, C. Cai, X.-F. Zang, Z. Iqbal, H. Zeng, D.-B. Kuang, L. Wang, H. Meier and D. Cao, *J. Mater. Chem. A*, 2015, **3**, 1333–1344.
44 C.-Y. Lo, D. Kumar, S.-H. Chou, C.-H. Chen, C.-H. Tsai, S.-H. Liu, P.-T. Chou and K.-T. Wong, *ACS Appl. Mater. Interfaces*, 2016, **8**, 27832–27842.
45 H. Meier, Z.-S. Huang and D. Cao, *J. Mater. Chem. C*, 2017, **5**, 9828–9837.
46 Z. Wang, Q. Chen, Y. Zou, J. Chen, Y. Luo, Y. Liu, S. Ding, P. Cai, J. Yuan and M. Liang, *Dyes Pigm.*, 2021, **187**, 109134.
47 Y. H. Lee, R. K. Chitumalla, B. Y. Jang, J. Jang, S. Thogiti and J. H. Kim, *Dyes Pigm.*, 2016, **133**, 161–172.
48 K. Zeng, W. Tang, C. Li, Y. Chen, S. Zhao, Q. Liu and Y. Xie, *J. Mater. Chem. A*, 2019, **7**, 20854–20860.
49 J. An, X. Yang, B. Cai, L. Zhang, K. Yang, Z. Yu, X. Wang, A. Hagfeldt and L. Sun, *ACS Appl. Mater. Interfaces*, 2020, **12**, 46397–46405.
50 S. M. Feldt, E. A. Gibson, E. Gabrielsson, L. Sun, G. Boschloo and A. Hagfeldt, *J. Am. Chem. Soc.*, 2010, **132**, 16714–16724.
51 S. C. Pradhan, A. Hagfeldt and S. Soman, *J. Mater. Chem. A*, 2018, **6**, 22204–22214.
52 M. Pazoki, U. B. Cappel, E. M. J. Johansson, A. Hagfeldt and G. Boschloo, *Energy Environ. Sci.*, 2017, **10**, 672–709.
53 Y. Wang, L. Yang, M. Xu, M. Zhang, Y. Cai, R. Li and P. Wang, *J. Phys. Chem. C*, 2014, **118**, 16441–16446.
54 R. Ambre, K.-B. Chen, C.-F. Yao, L. Luo, E. W.-G. Diau and C.-H. Hung, *J. Phys. Chem. C*, 2012, **116**, 11907–11916.
55 W. Zhang, X. Dai, X. Liao, X. Zang, H. Zhang, X. Yin, C. Yu, C. Ke and Y. Hong, *Sol. Energy*, 2020, **212**, 220–230.
56 J. J. P. Stewart, *J. Mol. Model.*, 2007, **13**, 1173–1213.
57 M. Korth, M. Pitoňák, J. Řezáč and P. Hobza, *J. Chem. Theory Comput.*, 2010, **6**, 344–352.
58 J. Bisquert, F. Fabregat-Santiago, I. Mora-Seró, G. Garcia-Belmonte and S. Giménez, *J. Phys. Chem. C*, 2009, **113**, 17278–17290.
59 S. Vijaya, G. Landi, H.-C. Neitzert and S. Anandan, *Phys. Chem. Chem. Phys.*, 2020, **22**, 18183–18191.
60 M. Kokkonen, P. Talebi, J. Zhou, S. Asgari, S. A. Soomro, F. Elsehrawy, J. Halme, S. Ahmad, A. Hagfeldt and S. G. Hashmi, *J. Mater. Chem. A*, 2021, **9**, 10527–10545.

